

Synchronized Ion Acceleration by Ultraintense Slow Light

A. V. Brantov,^{1,2} E. A. Govras,^{1,2} V. F. Kovalev,^{2,3} and V. Yu. Bychenkov^{1,2}

¹*P. N. Lebedev Physics Institute, Russian Academy of Science, Moscow 119991, Russia*

²*Center for Fundamental and Applied Research, Dukhov Research Institute of Automatics (VNIIA), Moscow 127055, Russia*

³*Keldysh Institute of Applied Mathematics, Russian Academy of Sciences, Moscow 125047, Russia*

(Received 12 October 2015; published 26 February 2016)

An effective scheme of synchronized laser-triggered ion acceleration and the corresponding theoretical model are proposed for a slow light pulse of relativistic intensity, which penetrates into a near-critical-density plasma, strongly slows, and then increases its group velocity during propagation within a target. The 3D particle-in-cell simulations confirm this concept for proton acceleration by a femtosecond petawatt-class laser pulse experiencing relativistic self-focusing, quantify the characteristics of the generated protons, and demonstrate a significant increase of their energy compared with the proton energy generated from optimized ultrathin solid dense foils.

DOI: 10.1103/PhysRevLett.116.085004

Many acceleration concepts using short relativistically intense laser pulses are applied for generating high-energy ions [1,2]. Most mechanisms of laser-triggered ion generation are tailored to a forward acceleration of ions from solid targets, but a new trend has recently appeared based on using low-density targets [3,4], which could be related to advanced materials such as aerogels, nanoporous carbon, etc. The hope is that for lasers with ~ 1 PW power they may increase ion energy compared with solid targets. The challenging way to accelerate ions up to ~ 1 GeV is ion wakefield acceleration [5,6], but this is a difficult task because heavy particles cannot be preaccelerated and trapped by the wakefield as easily as electrons can [7,8].

For an effective acceleration in a rare plasma, similarly to electron wakefield acceleration, ions must be preaccelerated up to a relativistic velocity. Several two-stage schemes for ion acceleration have been proposed [9–12] using thin foil or microdroplets to preaccelerate ions (in particular, due to a radiation-pressure-dominated regime [13]), which can then be trapped and accelerated in a gas plasma. For this scenario, an exawatt-class laser is required. Laser energy is less demanding for a near-critical-density plasma used for ion acceleration at a second stage [14]. The laser snowplow effect in a near-critical-density plasma, where the electrostatic potential generated by the laser pulse accelerates and reflects ions, has been discussed in Refs. [5,15], similarly to collisionless electrostatic shock acceleration [16].

A pulse of intense slow light can trap slow or even at-rest ions in its ponderomotive sheath potential and accelerate ions. But a laser pulse with a group velocity significantly less than the speed of light cannot accelerate ions to a high energy ~ 1 GeV until the group velocity itself starts to increase during pulse propagation. In this Letter, we propose a new scheme for ion acceleration by a laser pulse from a target with an electron density near the threshold of

relativistic transparency. The key point is the capability for the laser pulse first to slow and then to increase its group velocity monotonically. Ions are accelerated on the up-going laser ponderomotive field similarly to electron acceleration on the down-going pulse ramp [17]. The monotonic increase of the pulse group velocity makes ions achieve a synchronized acceleration by slow light (SASL). We present an analytic model and 3D particle-in-cell (PIC) simulations that demonstrate how SASL works when the increase of the pulse group velocity in a near-critical-density plasma is due to relativistic self-focusing, channeling, and evolution of electron density. Schemes of something similar to particle-field synchronization have been proposed by Katsouleas [18] (accelerated electrons and wakefield in a rare plasma with a decreasing density) and by Bulanov *et al.* [19] (accelerated ions and electromagnetic field in the radiation-pressure regime).

A relativistic laser pulse can propagate in a plasma with the electron density $n_e/\gamma n_c < 1$, where n_c is the electron critical plasma density and γ is the electron gamma factor. The group velocity $v_g = c\sqrt{1 - n_e/\gamma n_c}$ (c is the speed of light) of the light pulse inside the plasma should be small for effective loading and trapping of the ions in a self-consistent ponderomotive sheath. This is possible only in a rather narrow range of target densities, $n_e \sim \gamma n_c$, which slow a laser pulse and allow only the very top of the pulse with a sufficiently large intensity to propagate. For a given laser intensity, we should correspondingly expect a substantial selectivity of the target density.

When the front of a laser pulse hits an overdense target ($n_e > \gamma n_c$), it penetrates to a skin depth $\sim c\sqrt{\gamma}/\omega_{pe}$ and pushes electrons by the ponderomotive force F_p . This force moves electrons deeper into the target, creating an electron density spike at the pulse front until F_p is balanced by the charge separation electric force (see, e.g., Refs. [20,21]), $-\nabla\Phi = eE \sim F_p$. The slower the pulse propagation, the

more accurate the estimate $eE = F_p$. To describe the SASL mechanism qualitatively, we adopt this equality and the widely used estimates $\Phi = m_e c^2 \gamma$ and $\gamma = \sqrt{1 + a^2(x, t)/2}$ for the ponderomotive potential and gamma factor, where a is the normalized amplitude of the laser vector potential. Initially, the scale length of the pulse intensity is the skin depth. It increases in time (as laser pulse intensity increases) and reaches a value $\sim c/\omega_0$, when the target becomes transparent for the near-peak intensity. The pulse starts propagating inside the target with a small group velocity $v_g \ll c$. In some specific cases, the group velocity can increase as the light penetrates deeper into the plasma, for example, as a result of relativistic self-focusing or a monotonic decrease of the target density from front to back. The ponderomotive electric sheath, which propagates in the plasma with the same group velocity, i.e., $\Phi = m_e c^2 \sqrt{1 + a^2(x - v_g t)/2}$, can trap some ions. If the rate of ponderomotive ion acceleration is close to the rate of the laser pulse acceleration, then the ions gain energy very efficiently. To justify this, we consider the equations of motion for a test ion (a proton, for definiteness) accelerated in the ponderomotive sheath

$$\frac{dp}{dt} = -\frac{d}{d\xi}\Phi(\xi), \quad \frac{dx}{dt} = v = \frac{p}{\sqrt{1 + p^2}}, \quad (1)$$

where the coordinates x and $\xi(x, t) = x - tv_g(t)$ are normalized to the characteristic pulse spatial width σ . The time t , the velocities v and v_g , the momentum p , and the sheath potential Φ are, respectively, normalized to σ/c , c , $m_p c$, and $m_e c^2/\rho$ ($\rho = m_e/m_p = 1/1836$).

Equation (1) describes a nonlinear oscillator and allows finite and infinite motion. Finite motion corresponds to ion reflection from the sheath as for acceleration by a collisionless shock wave [22]. For example, in the nonrelativistic limit $p \ll 1$, Eq. (1) has a well-known solution in the case of a constant group velocity $v_g = v_{g,0}$. If the initial proton velocity p_0 is less than $v_{g,0}$, i.e., the parameter $\delta v = p_0 - v_{g,0} < 0$ and $\Phi_{\max} = \rho \sqrt{1 + a_0^2/2} > (\delta v)^2/2$ (cf. Ref. [14]), then the proton is reflected by the ponderomotive potential and attains the velocity $2v_{g,0} - p_0$. In the case of an accelerating pulse, i.e., a time-dependent group velocity $v_g(t)$, the proton after being reflected can be caught by the pulse and reflected again. Each reflection increases the proton momentum in accordance with the instantaneous pulse velocity. These multiple reflections significantly accelerate the ion if it is in phase with the group velocity increase. We call this the SASL case.

As an example, we consider a linearly increasing group velocity $v_g(t) = v_{g,0} + w_0 t$ in the nonrelativistic case $p \ll 1$. The corresponding analytic solution $\xi(t)$ is given in quadrature by the expression

$$t - t_0 = \pm \int_{\xi_0}^{\xi} \frac{dz}{\sqrt{\dot{\xi}_0^2 + 2[\Phi(\xi_0) - \Phi(z)] - 4w_0(z - \xi_0)}}, \quad (2)$$

where $\xi_0 = \xi(t_0)$ and $\dot{\xi}_0 = \dot{\xi}(t_0)$. Equation (2) describes the ion motion starting at the instant t_0 from the position corresponding to $(\xi_0, \dot{\xi}_0)$. For finite (oscillatory) motion, there are two return points in the pulse reference frame where $\dot{\xi} = 0$. In the lab frame, one of the return points corresponds to the maximum distance of the ion from the sheath (the point with the maximum coordinate ξ), and the second return point is the electrostatic sheath reflection point. The direction of ion motion from one return point (or the initial point corresponding to $t_0 = 0$, $\xi_0 = x_0$, $\dot{\xi}_0 = \delta v$) to the other defines the proper sign choice in Eq. (2).

To illustrate the obtained analytic solution given by Eq. (2), we present phase plots for the case of a Gaussian spatial profile of the accelerating ponderomotive electric field. Figure 1 clearly demonstrates ion oscillations with multiple reflections from the pulse (SASL) for a sufficiently small pulse acceleration w_0 , which allows an effective energy increase. The existence of two roots of the equation $\dot{\xi} = 0$ defines a restriction on w_0 for which SASL is allowed:

$$w_0 \leq \frac{1}{2(x_0 - \xi_*)} \left[\Phi(\xi_*) - \Phi(x_0) - \frac{(\delta v)^2}{2} \right], \quad (3)$$

where the value ξ_* is defined from the solution of the equation $\Phi(\xi_*) - \Phi(x_0) = (\delta v)^2/2 + (\xi_* - x_0)\Phi'(\xi_*)$. For a given w_0 , we can find the domain of initial values $(x_0, \delta v)$ satisfying the SASL condition. Correspondingly, there is a maximum value of w_0 above which a synchronized ion-pulse motion is impossible. The dependence of the maximum pulse acceleration $\max(w_0)$ on the maximum laser pulse amplitude is shown in Fig. 2. The steep increase of $\max(w_0)$ with the laser field amplitude for sufficiently high

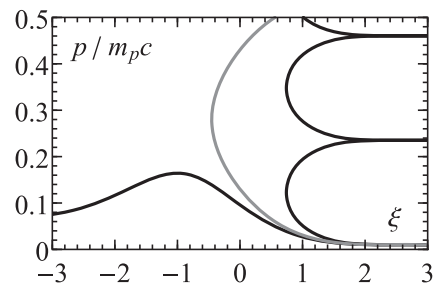


FIG. 1. Phase space for an ion starting from $x_0 = 3$ with $\delta v = 0.01$. The gray curve ($w_0 \approx 0.028$) separates the finite and infinite regimes illustrated by the examples $w_0 = 0.001$ (at the right) and $w_0 = 0.004$ (at the left). The laser amplitude is $a_0 = 60$.

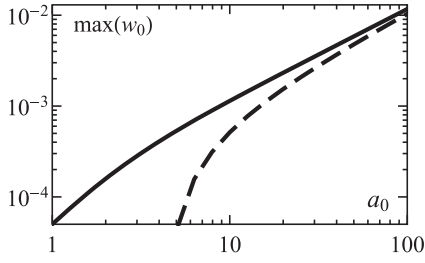


FIG. 2. Maximum pulse acceleration above which a synchronized ion-pulse motion is impossible for $\delta v = 0$ (solid curve) and $\delta v = \pm 0.05$ (dashed curve).

$|\delta v|$ (i.e., $\delta v = \pm 0.05$; see the dashed curve in Fig. 2), in fact, demonstrates the existence of the SASL threshold; i.e., $(\delta v)^2/2 = \Phi_{\max} - \Phi(x_0)$.

From the first integral of Eq. (2), $\dot{\xi}^2/2 - \dot{\xi}_0^2/2 = \Phi(\xi_0) - \Phi(\xi) - 2w_0(\xi - \xi_0)$, we can estimate the proton energy increase. For protons initially at rest, the proton energy evolves as $\varepsilon = 2w_0(vt - x) + \Phi(\xi_0) - \Phi(\xi)$. In average, an ion moves together with the laser pulse and has a constant acceleration $x \sim w_0 t^2$, which results in an ion energy increase as $w_0^2 t^2$. However, such a rapid energy gain is only in the nonrelativistic limit. The nonrelativistic solution presented can describe ion acceleration only for $\varepsilon \ll m_p c^2$, while the SASL can yield a much higher ion energy. For a linear time dependence of v_g , the relativistic nonlinearity in Eq. (1) sooner or later breaks the SASL. To describe the relativistic regime more accurately, we must take the natural saturation of the group velocity at the speed of light into account. We present the corresponding illustration in Fig. 3 as a result of solving Eq. (1) numerically for the saturating group velocity $v_g = w_0 t / (1 + w_0 t)$, which shows continuous particle acceleration up to relativistic energies. The average energy of accelerated protons increases almost linearly with the propagation distance and highlights the SASL advantage.

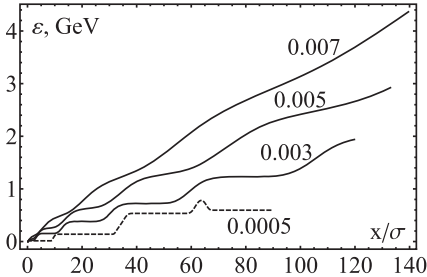


FIG. 3. The proton energy gain for $x_0 = 1$ and $p_0 = 0$ versus the propagation length for the ponderomotive potential characterized by $a_0 = 60$ and $v_g = w_0 t / (1 + w_0 t)$, where $w_0 = 0.003, 0.005, 0.007$ (the numbers near the curves). The dashed curve shows the energy gain for $a_0 = 60$ and $v_g = 0.0005t$.

Other physical effects accompanying the laser pulse propagation, for example, pulse depletion, deformation of the pulse shape, violation of the ideal electron equilibration $eE \sim F_p$, complicate the theoretical model. They might degrade the theoretical estimates of the ion energy gain, but the basic principle of the SASL should remain. To confirm this, we performed 3D PIC simulations for short (30 fs FWHM duration) and tightly focused (4λ FWHM spot size) Gaussian laser pulses using the code MANDOR [23]. The peak laser intensities in the focal spot were varied from $I = 5 \times 10^{20}$ W/cm² (3 J) to $I = 10^{22}$ W/cm² (60 J). The pulse was focused on the front side of a thin CH₂ plasma target, which consists of electrons, hydrogen ions, and fully ionized carbon ions (C⁶⁺). The target densities were decreased from the solid mass density 1.1 g/cm³ ($n_e = 200n_c$) to the density 5.5 mg/cm³ ($n_e = n_c$). The target thickness l was varied from 3 nm to 30 μ m.

Several runs with different target densities and thicknesses were performed to find the maximum proton energy. The results of simulations are shown in Fig. 4 (for 3 and 30 J lasers) by the dots, which correspond to those target thicknesses which maximize proton energy. Figure 4 demonstrates an existence of certain resonant (optimal) densities providing enhanced proton acceleration inside a target. Using a 3 J laser pulse does not effectively synchronize the protons and laser pulse, although there is some proton energy increase (up to 30%) during acceleration inside a target. An effective SASL acceleration occurs at considerably higher pulse energy. We demonstrate this with the example of proton acceleration by a petawatt-class laser (30 J). For a target with an optimal density of $20n_c$, a significant increase of the maximum proton energy was found and $\sim 80\%$ of the total energy is acquired inside the target. For such a density, the front wing of the laser pulse does not penetrate into the target, but the near-peak intensity does penetrate and propagates inside the plasma with an increasing group velocity (solid curve in the inset in Fig. 5), which can be roughly approximated as $v_g = c(0.04 + 0.0045\omega t)$ (dashed line in this inset). The laser-induced electrostatic sheath field corresponds well to

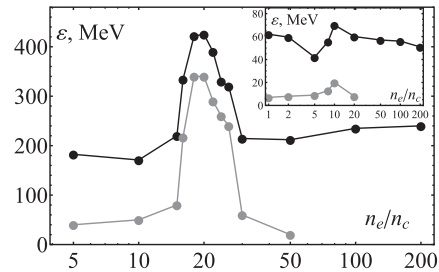


FIG. 4. Maximum proton energy versus target electron density for optimal target thickness (black dots) for laser energies of 30 and 3 J (inset). Gray dots show maximum energy gained inside target.

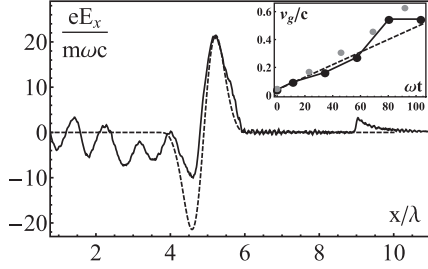


FIG. 5. An electrostatic field inside a $6\ \mu\text{m}$ width target and pulse velocity (inset) for $n_e = 20n_c$ and a 30 J laser pulse. The target is placed from $x = 3\lambda$ to $x = 9\lambda$. The dashed curve corresponds to proposed fits. Gray points in inset are the maximum proton velocity from 3D simulation.

the Gaussian-shape potential with $a_0 = 100$ and $\sigma = 2c/\omega$ (the dashed curve in Fig. 5). For a 30 J laser and $n_e = 20n_c$, the increase of the pulse group velocity is sufficiently small ($w_0 = 0.009$), which is favorable for an effective trapping of the protons in the ponderomotive potential (cf. Fig. 2). The protons gain significant energy as a result of the SASL mechanism. Synchronized motion of the proton front and ponderomotive sheath is clearly seen in Fig. 5 (cf. black and gray dots in the inset). We estimated the energy gain of the test protons (initially at rest or weakly preaccelerated) as the solution of Eq. (1). At the distance of $6\ \mu\text{m}$, the protons gain energy of 350–400 MeV (see Fig. 6), which is consistent with the PIC simulation result (black dots in Fig. 6). For $x > 6\lambda$, the electrostatic potential overtakes the protons and decelerates them as a result of the transition to the relativistic regime and violation of the phasing in. However, for petawatt-class pulses, the targets of multi- μm thicknesses are weakly sensitive to such dephasing. Simulation shows that target which is 5 times thicker than the optimum target gives only a 12% decrease of proton energy for the laser pulse with energy of 30 J. Such a pulse can accelerate 10^9 protons with the energy in excess of 300 MeV. More results on maximum proton energy for different pulse energies are shown in Table I, where $\delta\epsilon/\epsilon$ quantifies which additional energy can be picked up with the SASL mechanism (last column).

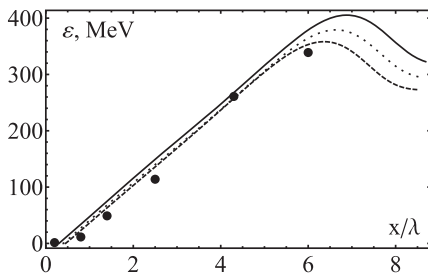


FIG. 6. Energy gain of test protons with $x_0 = 0.4\lambda$ and $p_0 = 0$ (dotted curve), $x_0 = 0.3\lambda$ and $p_0 = 0.01$ ($\epsilon_0 = 50\ \text{keV}$) (solid curve), and $x_0 = 0.35\lambda$ and $p_0 = 0$ (dashed curve). Black dots correspond to the results of PIC simulation.

TABLE I. Optimal condition for SASL mechanism realization.

| Intensity ($10^{21}\ \text{W}/\text{cm}^2$) | Density (n_c) | Thickness (μm) | Energy (MeV) | $\delta\epsilon/\epsilon$ (%) |
|--|----------------------|--------------------------------|-----------------|----------------------------------|
| 0.5 | 10 | 1–3 | 70 | 30% |
| 1 | 13–14 | 2–4 | 110 | 50% |
| 2 | 14–18 | 4–8 | 210 | 70% |
| 5 | 18–22 | 6–30 | 420 | 100% |
| 10 | 20–26 | 6–30 | 610 | 100% |

In conclusion, we have proposed a new model of proton acceleration by an ultraintense slow light pulse interacting with low-density targets. The key points of this mechanism are to stop the laser pulse at the front of the target and then accelerate the infiltrating intense part of the pulse inside a plasma at the same rate as the proton energy increase in a ponderomotive potential to achieve synchronized acceleration by slow light (SASL). In the case considered, the linearly polarized laser pulse propagates and increases its group velocity as a result of a relativistic self-induced transparency. Another scheme of pulse acceleration could be based on using a plane target with its density decreasing from front to back. The SASL regime is challenging for low-density material applications and will require production of lightweight foils with fully variable and controllable parameters. Such foils should typically have a multimicron thickness that makes them more robust in laser acceleration experiments in contrast to nanoscale solid dense foils, which require an extremely clean pulse shape. Finally, we note that our simulations with low-density targets have demonstrated more than a twofold increase of proton energy compared with the case of solid dense foils of optimal submicron thickness [24].

This research was funded by a grant from the Russian Science Foundation (Project No. 14-12-00194).

- [1] H. Daido, M. Nishiuchi, and A. S. Pirozhkov, *Rep. Prog. Phys.* **75**, 056401 (2012).
- [2] A. Macchi, M. Borghesi, and M. Passoni, *Rev. Mod. Phys.* **85**, 751 (2013).
- [3] M. Passoni, A. Zani, A. Sgattoni, D. Dellasega, A. Macchi, I. Prencipe, V. Floquet, P. Martin, T. V. Liseykina, and T. Ceccotti, *Plasma Phys. Controlled Fusion* **56**, 045001 (2014).
- [4] J. H. Bin, W. J. Ma, H. Y. Wang, M. J. V. Streeter, C. Kreuzer, D. Kiefer, M. Yeung, S. Cousens, P. S. Foster, B. Dromey *et al.*, *Phys. Rev. Lett.* **115**, 064801 (2015).
- [5] O. Shorokhov and A. Pukhov, *Laser Part. Beams* **22**, 175 (2004).
- [6] B. Shen, Y. Li, M. Y. Yu, and J. Cary, *Phys. Rev. E* **76**, 055402 (2007).
- [7] E. Esarey, C. Schroeder, and W. Leemans, *Rev. Mod. Phys.* **81**, 1229 (2009).
- [8] A. Pukhov and J. Meyer-ter Vehn, *Appl. Phys. B* **74**, 355 (2002).

- [9] B. Shen, X. Zhang, Z. Sheng, M. Y. Yu, and J. Cary, *Phys. Rev. ST Accel. Beams* **12**, 121301 (2009).
- [10] L.-L. Yu, H. Xu, W.-M. Wang, Z.-M. Sheng, B.-F. Shen, W. Yu, and J. Zhang, *New J. Phys.* **12**, 045021 (2010).
- [11] X. Zhang, B. Shen, L. Ji, F. Wang, M. Wen, W. Wang, J. Xu, and Y. Yu, *Phys. Plasmas* **17**, 123102 (2010).
- [12] F. L. Zheng, S. Z. Wu, C. T. Zhou, H. Y. Wang, X. Q. Yan, and X. T. He, *Europhys. Lett.* **95**, 55005 (2011).
- [13] T. Esirkepov, M. Borghesi, S. V. Bulanov, G. Mourou, and T. Tajima, *Phys. Rev. Lett.* **92**, 175003 (2004).
- [14] H. Y. Wang, X. Q. Yan, and M. Zepf, *Phys. Rev. ST Accel. Beams* **18**, 021302 (2015).
- [15] A. A. Sahai, F. S. Tsung, A. R. Tableman, W. B. Mori, and T. C. Katsouleas, *Phys. Rev. E* **88**, 043105 (2013).
- [16] D. Haberberger, S. Tochitsky, F. Fiuza, C. Gong, R. A. Fonseca, L. O. Silva, W. B. Mori, and C. Joshi, *Nat. Phys.* **8**, 95 (2011).
- [17] C. K. Lau, P. C. Yeh, O. Luk, J. McClenaghan, T. Ebisuzaki, and T. Tajima, *Phys. Rev. ST Accel. Beams* **18**, 024401 (2015).
- [18] T. Katsouleas, *Phys. Rev. A* **33**, 2056 (1986).
- [19] S. V. Bulanov, E. Y. Echkina, T. Z. Esirkepov, I. N. Inovenkov, M. Kando, F. Pegoraro, and G. Korn, *Phys. Rev. Lett.* **104**, 135003 (2010).
- [20] F. Cattani, A. Kim, D. Anderson, and M. Lisak, *Phys. Rev. E* **62**, 1234 (2000).
- [21] E. Siminos, M. Grech, S. Skupin, T. Schlegel, and V. T. Tikhonchuk, *Phys. Rev. E* **86**, 056404 (2012).
- [22] R. Z. Sagdeev, in *Reviews of Plasma Physics*, edited by M. A. Leontovich (Consultants Bureau, New York, 1966), Vol. 4, p. 23.
- [23] D. V. Romanov, V. Y. Bychenkov, W. Rozmus, C. E. Capjack, and R. Fedosejevs, *Phys. Rev. Lett.* **93**, 215004 (2004).
- [24] A. V. Brantov, E. A. Govras, V. Y. Bychenkov, and W. Rozmus, *Phys. Rev. ST Accel. Beams* **18**, 021301 (2015).